Research Article
Experimental and Translational Hepatology

JOURNAL
OF HEPATOLOGY

Exploring the impact of the PNPLA3 I148M variant on primary human hepatic stellate cells using 3D extracellular matrix models

Authors

Elisabetta Caon, Maria Martins, Harry Hodgetts, …, Giuseppe Mazza, Massimo Pinzani, Krista Rombouts

Correspondence

k.rombouts@ucl.ac.uk (K. Rombouts).

Graphical abstract

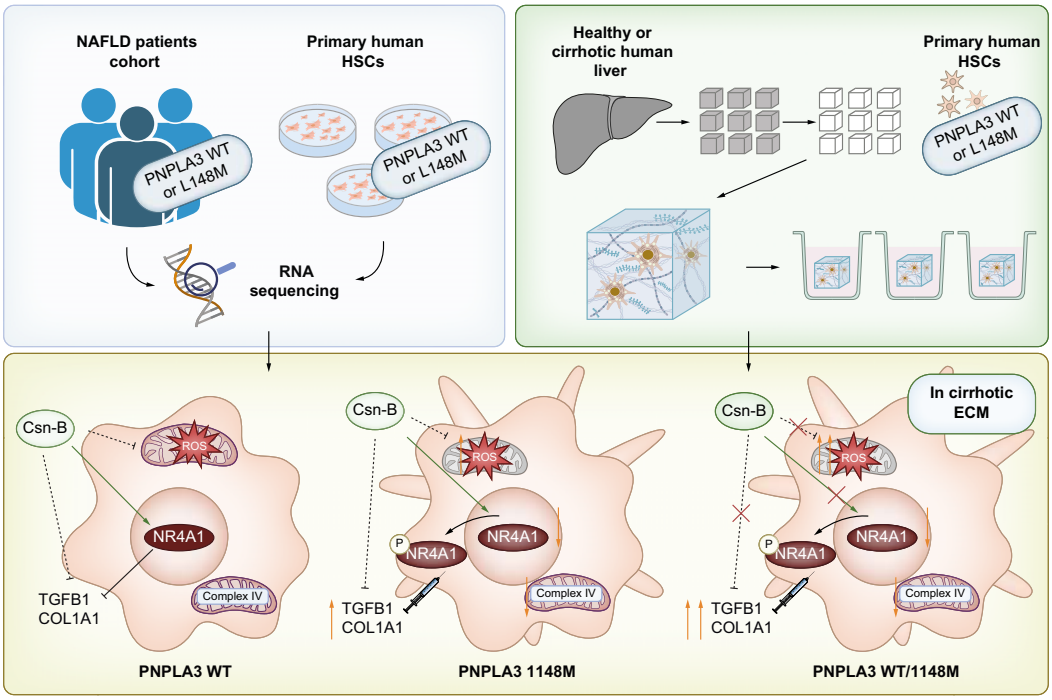

Highlights

- Transcriptomic analyses were performed to investigate the involvement of the *PNPLA3* I148M variant in the pro-fibrogenic features of HSCs.
- HSCs carrying the *PNPLA3* I148M variant are characterized by mitochondrial dysfunction and decreased antioxidant capacity.
- HSCs carrying the *PNPLA3* I148M variant have increased TGFB1 signalling which reduces the antifibrotic activity of its endogenous inhibitor NR4A1.
- The ECM of cirrhotic liver further exacerbates the effects of the *PNPLA3* I148M variant on HSC behaviour.

Impact and implications

Hepatic stellate cells (HSCs) play a key role in the fibrogenic process associated with chronic liver disease. The *PNPLA3* genetic mutation has been linked with increased risk of fibrogenesis, but its role in HSCs requires further investigation. Here, by using comparative transcriptomics and a novel 3D *in vitro* model, we demonstrate the impact of the *PNPLA3* genetic mutation on primary human HSCs' behaviour, and we show that it affects the cell's mitochondrial function and antioxidant response, as well as the antifibrotic gene *NR4A1*. Our publicly available transcriptomic data, 3D platform and our findings on NR4A1 could facilitate the discovery of targets to develop more effective treatments for chronic liver diseases.

https://doi.org/10.1016/j.jhep.2024.01.032
 J. Hepatol. 2024, 80, 941–956

Research Article
Experimental and Translational Hepatology

JOURNAL
OF HEPATOLOGY

Exploring the impact of the PNPLA3 I148M variant on primary human hepatic stellate cells using 3D extracellular matrix models

Elisabetta Caon[1,†], Maria Martins[1], Harry Hodgetts[1], Lieke Blanken[1], Maria Giovanna Vilia[1], Ana Levi[1], Kessarin Thanapirom[1], Walid Al-Akkad[1], Jeries Abu-Hanna[2], Guido Baselli[6], Andrew R. Hall[7,10], Tu Vinh Luong[7,10], Jan-Willem Taanman[3], Michele Vacca[4,5], Luca Valenti[6,8], Stefano Romeo[9], Giuseppe Mazza[1], Massimo Pinzani[1], Krista Rombouts[1,*]

Journal of Hepatology **2024**. vol. 80 | 941–956

Background & Aims: The *PNPLA3* rs738409 C>G (encoding for I148M) variant is a risk locus for the fibrogenic progression of chronic liver diseases, a process driven by hepatic stellate cells (HSCs). We investigated how the PNPLA3 I148M variant affects HSC biology using transcriptomic data and validated findings in 3D-culture models.
Methods: RNA sequencing was performed on 2D-cultured primary human HSCs and liver biopsies of individuals with obesity, genotyped for the PNPLA3 I148M variant. Data were validated in wild-type (WT) or PNPLA3 I148M variant-carrying HSCs cultured on 3D extracellular matrix (ECM) scaffolds from human healthy and cirrhotic livers, with/without TGFB1 or cytosporone B (Csn-B) treatment.
Results: Transcriptomic analyses of liver biopsies and HSCs highlighted shared PNPLA3 I148M-driven dysregulated pathways related to mitochondrial function, antioxidant response, ECM remodelling and TGFB1 signalling. Analogous pathways were dysregulated in WT/PNPLA3-I148M HSCs cultured in 3D liver scaffolds. Mitochondrial dysfunction in PNPLA3-I148M cells was linked to respiratory chain complex IV insufficiency. Antioxidant capacity was lower in PNPLA3-I148M HSCs, while reactive oxygen species secretion was increased in PNPLA3-I148M HSCs and higher in bioengineered cirrhotic *vs.* healthy scaffolds. TGFB1 signalling followed the same trend. In PNPLA3-I148M cells, expression and activation of the endogenous TGFB1 inhibitor NR4A1 were decreased: treatment with the Csn-B agonist increased total NR4A1 in HSCs cultured in healthy but not in cirrhotic 3D scaffolds. NR4A1 regulation by TGFB1/Csn-B was linked to Akt signalling in PNPLA3-WT HSCs and to Erk signalling in PNPLA3-I148M HSCs.
Conclusion: HSCs carrying the PNPLA3 I148M variant have impaired mitochondrial function, antioxidant responses, and increased TGFB1 signalling, which dampens antifibrotic NR4A1 activity. These features are exacerbated by cirrhotic ECM, highlighting the dual impact of the PNPLA3 I148M variant and the fibrotic microenvironment in progressive chronic liver diseases.

Introduction

Chronic liver disease (CLD) is a leading cause of death worldwide with an estimated number of cases of around 1.5 billion.[1] The most common causes are non-alcoholic liver disease (NAFLD) or MAFLD (metabolic dysfunction-associated fatty liver disease) (59%),[2] chronic HBV (29%) and HCV (9%) infections, and alcohol-related liver disease (ALD) (2%).[1] NAFLD affects approximately 25% of the world's adult population,[3] with a percentage of patients progressing to non-alcoholic steatohepatitis (NASH) which can then lead to cirrhosis and hepatocellular carcinoma.[4] Fibrosis stage has been identified as the most important predictor of prognosis in patients with NAFLD.[5] Liver fibrosis is defined as the progressive deposition of fibrillar extracellular matrix (ECM) associated with gradual nodular regeneration of the liver parenchyma leading to cirrhosis.[6,7] The excessive deposition of fibrillary ECM is mediated by hepatic stellate cells (HSCs),[8] liver-specific pericytes which undergo a phenotypical modulation into myofibroblasts in response to several micro-environmental disturbances.[9] Among these are the release of cytokines and chemokines by platelets and inflammatory cells,[10] the secretion of damage-associated reactive oxygen species (ROS), the generation of lipid peroxides and apoptotic bodies by damaged hepatocytes[11,12] and a major disturbance of ECM homeostasis

Keywords: Hepatic stellate cells; PNPLA3; fibrosis; 3-dimensional (3D) models; extracellular matrix (ECM); transcriptomics; mitochondrial dysfunction; oxidative stress; TGFB1; NR4A1 (Nur77).
Received 8 December 2022; received in revised form 24 January 2024; accepted 27 January 2024; available online 15 February 2024
* Corresponding author. Address: Regenerative Medicine and Fibrosis Group, Institute for Liver and Digestive Health, University College London, Royal Free Campus, London, UK.
E-mail address: k.rombouts@ucl.ac.uk (K. Rombouts).
† Author is deceased.
https://doi.org/10.1016/j.jhep.2024.01.032

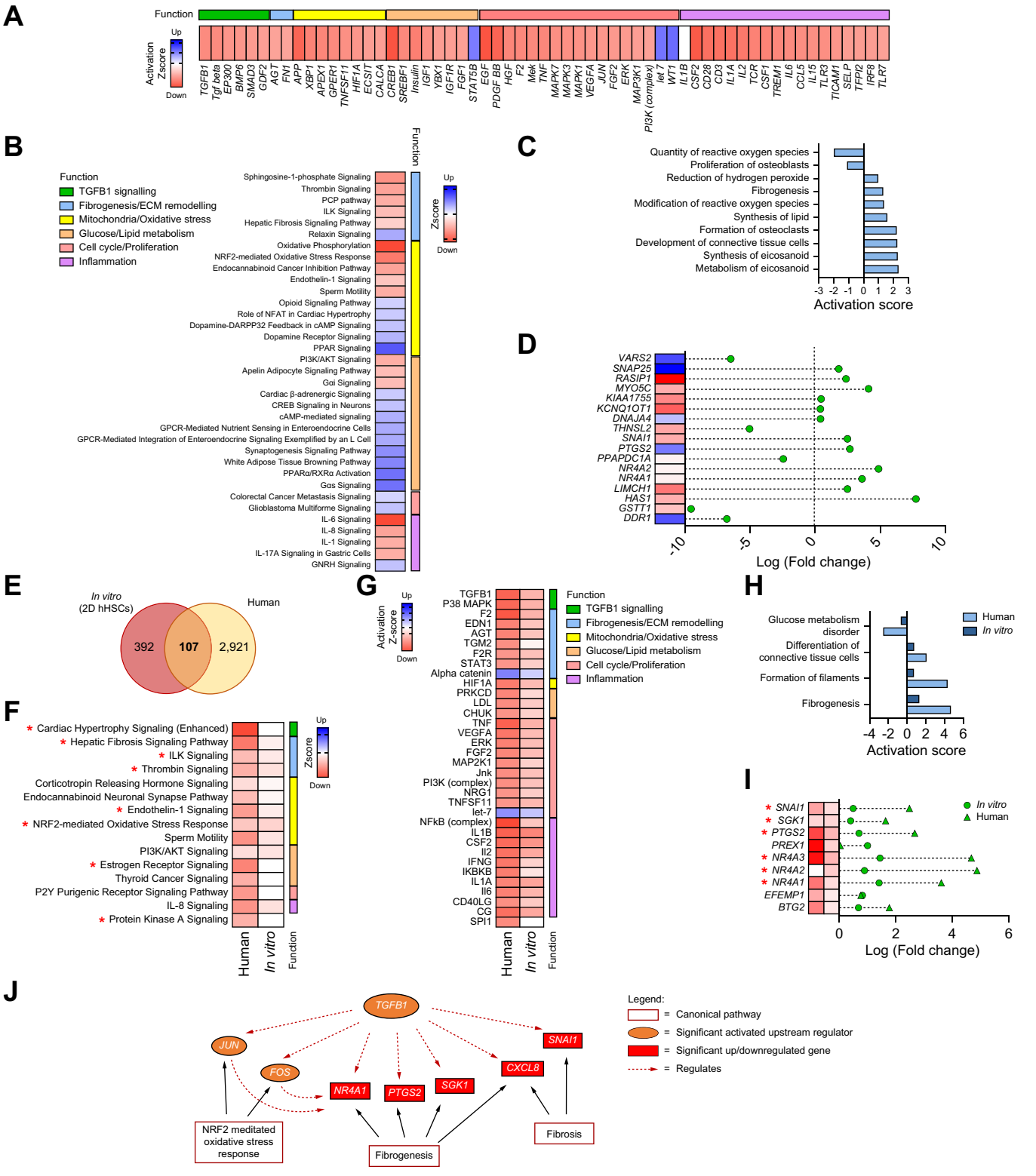

Fig. 1. Gene expression profiled by NGS and analysed by IPA of *in vitro*-cultured primary human HSCs and human biopsies genotyped for PNPLA3-WT-I148M mutations. IPA of *in vitro*-cultured primary human HSCs (n = 3 per genotype) stratified according to carriage of the PNPLA3-I148M variant. (A-B) Significantly enriched (A) upstream regulators predicted as activated (red) or inhibited (blue) (-2.25 ≤ Z-score ≥ 2.25, p <0.05) or (B) canonical pathways predicted as up- or downregulated (-0.5 ≤ Z-score ≥ 0.5, p <0.05). (C) Selection of significantly enriched biofunctions (-3 ≤ Z-score ≥ 3, p <0.05). (D) Major upregulated or downregulated target genes identified by NGS, p <0.05. Comparative IPA of *in vitro*-cultured primary human HSCs and human biopsies of patients (n = 60 WT and n = 56 I148M) stratified according to carriage of the I148M. (E) Comparison of transcriptomic data (NGS), showing shared number of significantly deregulated genes (p <0.05). (F–H) Comparative analysis of shared (F) significant canonical pathways. (-1 ≤ Z-score ≥ 1 for at least one dataset (human or *in vitro*) and going in the same direction for the other dataset, p ≤0.05, red asterisk indicates regulation by TGFB1) or (G) predicted upstream regulators (-4 ≤ Z-score ≥ 4 for at least one dataset (human or *in vitro*) and

in the space of Disse.[13] Genetic variants are a key determinant of the risk of development and progression of NAFLD.[14] Among them, the most robustly characterized and the one that accounts for the largest fraction of disease heritability[15] and susceptibility to develop steatohepatitis[16] is the I148M variant of the *PNPLA3* gene. Patatin-like phospholipase domain-containing 3 (PNPLA3, also called adiponutrin, ADPN) is a membrane-bound protein with lipase and transacylase activity towards triglycerides/phospholipids in hepatocytes and retinyl esters in HSCs.[17,18] *PNPLA3* is highly expressed in HSCs, where it is regulated by retinol and lipid homeostasis.[19] Several studies have proven the association between *PNPLA3* I148M and the development and severity of liver fibrosis, which might be at least partially independent from the predisposition to hepatic fat accumulation. Further, the *PNPLA3* I148M variant has been associated with hepatocellular carcinoma development[20–22] and previous studies have shown how the *PNPLA3* I148M variant facilitates HSC activation and how its expression is associated with a pro-fibrogenic, pro-inflammatory myofibroblast-like phenotype compared to wild-type *PNPLA3*.[23,24] While the presence of the *PNPLA3* I148M variant in HSCs has been associated with a deregulation of Yap signalling[25] and cholesterol metabolism,[26] a comprehensive study of the different mechanisms driving the progression of liver disease via *PNPLA3* variants has still to be provided. An obstacle to the analysis of the effects of the *PNPLA3* variant is the lack of adequate pre-clinical models. Although genetically modified mouse models carrying the PNPLA3 I148M variant have been generated,[27–29] PNPLA3 expression is highest in adipose tissue in mice,[30] whereas it is highest in the liver in humans.[31] Meanwhile, the most commonly used human cell lines (HepG2 and LX2) are already carriers of the *PNPLA3* I148M mutation, thus hampering the possibility of observing differences between a wild-type and mutant genotype.[32] In addition, the complex remodelling of the tissue microenvironment and cellular organization observed during liver fibrosis progression[33] can hardly be replicated in a classic 2D plastic culture dish. Among the newly developed models, human-derived liver 3D ECM scaffold cultures can recapitulate the tissue microarchitecture, ECM microenvironment and stiffness of both the healthy and cirrhotic human liver as we previously demonstrated.[34–37]

The aim of this study was to unravel the main HSC-related mechanisms driving the progression of liver disease in carriers of the *PNPLA3* I148M variant, by using transcriptomic analysis of patient-isolated human HSCs genotyped for *PNPLA3*. Selection of the main pathways modulated by the *PNPLA3* variant in HSCs, but also important for the overall progression of liver disease, was achieved by combining transcriptomic data from HSCs with data from whole biopsies of patients with NAFLD. Targets were validated using a 3D *in vitro* model of HSCs recapitulating the microenvironment of healthy and cirrhotic human livers.

Materials and methods

Please refer to the supplementary materials and methods section for more detailed descriptions.

Study population

The cohort was formed of 116 individuals with obesity previously characterized in the study by Baselli and colleagues.[38] Briefly, liver biopsy was performed by needle gauge during bariatric surgery. Steatosis was graded based on the percentage of affected hepatocytes; disease activity was assessed according to the NAFLD activity score; fibrosis was staged according to the recommendations of the NAFLD clinical research network.[39] A complete overview of the clinical features of the patients is provided in Table S2.

Primary human HSC isolation and culture

Human primary HSCs were isolated according to Rombouts *et al.*, and cells were isolated from normal human liver (*i.e.*, without inflammation and fibrosis), obtained after wedge section surgery in patients with liver metastasis from extrahepatic cancers (REC reference 21/WA/0388) (Table S6).[40] Cells were cultured in Iscove's Modified DMEM (Thermo Fisher Scientific, Watlham, USA), supplemented with 20% foetal bovine serum (Thermo Fisher Scientific, Watlham, USA), 2 mM Glutamine, 1X non-essential amino acids, 1.0 mM sodium pyruvate, 1X antibiotic-antimycotic (Life Technologies, Carlsbard, USA), and maintained under standard conditions in a humidified incubator under 5% CO_2 in air at 37 °C. Medium was refreshed twice a week and cells were passaged when subconfluent with 1X Trypsin (Gibco, Thermo Fisher Scientific, Watlham, USA). Experiments were performed on cell preparations used between passage 5 and 8.

Preparation of 3D human liver scaffolds and primary human HSC culture

Livers were obtained after approval by the UCL Royal Free BioBank Ethical Review Committee (NRES Rec Reference: 21/WA/0388). Informed consent was obtained for each donor and confirmed via the NHSBT ODT organ retrieval pathway. Healthy human livers were retrieved for transplantation but judged unsuitable due to prolonged cold ischemic time, the presence of extrahepatic cancer, or other significant extrahepatic diseases in donors or recipients. Cirrhotic liver was explanted from a patient with alcohol-related cirrhosis. Healthy liver was defined if there was no evidence of fibrosis and fat accumulation. 3D human liver scaffolds were prepared (Table S1) and quality control (Fig. S4) was performed according to the methodologies developed by Mazza G and colleagues.[35,36] 3D human liver scaffolds were then sterilized using 0.1% peracetic acid (Sigma-Aldrich, St. Louis, USA) and repopulated with primary HSCs as previously described.[35]

going in the same direction for the other dataset, $p \leq 0.05$) or (H) Biofunctions ($-4 \leq$ Z-score ≥ 4 for at least one group and going in the same direction for other groups, $p \leq 0.05$). (I) Major upregulated or downregulated target genes identified by NGS, $p < 0.05$. Red asterisk indicates regulation by TGFB1. (J) Schematic representation of the upstream regulator, canonical pathways and target genes highlighted by IPA and selected for further investigation. HSCs, hepatic stellate cells; IPA, Ingenuity Pathway Analysis; NGS, next-generation sequencing; WT, wild-type.

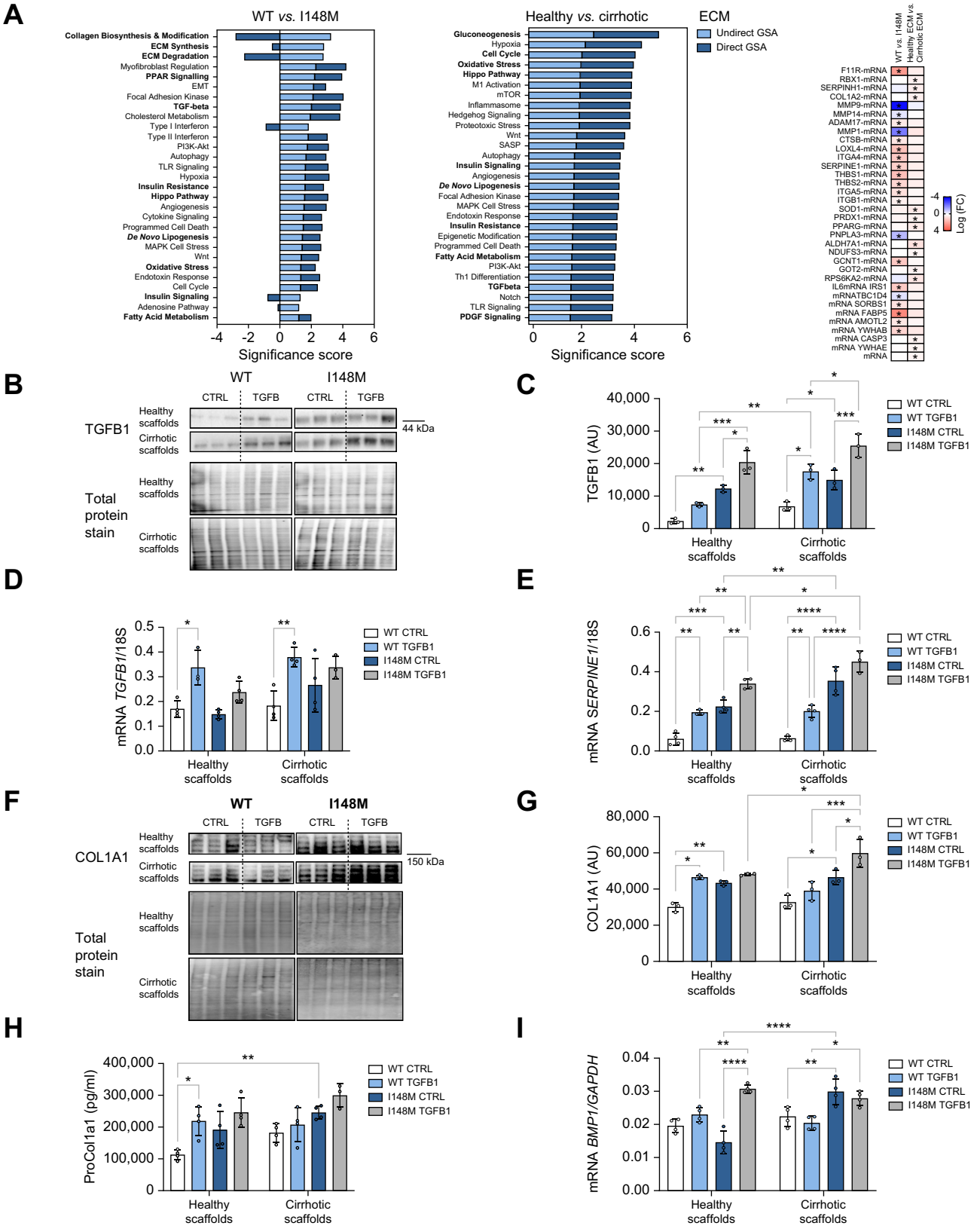

Fig. 2. Characterization of the 3D model of *PNPLA3* WT or I148M HSCs cultured on healthy or cirrhotic human liver decellularized scaffolds. (A) Nanostring nCounter RNA analysis for human fibrosis, showing list of up and downregulated pathways in PNPLA3-I148M *vs.* WT HSCs or HSCs cultured on cirrhotic ECM *vs.* healthy ECM, analysed by GSA (undirect or direct) (left), and heatmap representing gene expression of single molecules in PNPLA3 I148M *vs.* WT HSCs or HSCs cultured on cirrhotic ECM *vs.* healthy ECM (right). *p <0.05, n = 2 donors for each *PNPLA3* genotype and n = 3 for each ECM type. Analysis of expression of genes and proteins in PNPLA3-I148M *vs.* WT HSCs cultured on healthy or cirrhotic human liver decellularized scaffolds for 14 days and treated with TGFB1 (5 ng/ml). (B,C) TGFB1

Data analysis and statistics

The statistical analysis was performed using GraphPad Prism 9.0c software for Windows (Graph Pad CA, USA). Values are expressed as mean (SD). Sample groups were tested for normal distribution utilizing the Shapiro-Wilk test. Statistical significance was analysed using Student's *t* test or one/two-way or three-way ANOVA with Tukey's multiple comparison test.

Results

Transcriptomic analysis of PNPLA3-WT and PNPLA3-I148M HSCs and human liver biopsies

To investigate the impact of the *PNPLA3* I148M variant on the fibrogenic phenotype of HSCs, primary human HSCs were isolated, genotyped and classified as *PNPLA3* rs738409 CC (wild-type – from now on referred to as PNPLA3-WT) or *PNPLA3* rs738409 CG (heterozygous mutant – from now on referred to as PNPLA3-I148M). Primary HSCs were cultured on plastic, and next-generation sequencing (NGS) of bulk transcriptome was used to study the biological processes modulated by the *PNPLA3* variant. Ingenuity Pathway Analysis (IPA) highlighted a wide number of significantly deregulated "Canonical Pathways", ranging from increased fibrogenesis, inflammation, metabolism, and proliferation. Deregulated pathways were independently validated with specific markers in an additional experiment where HSCs were cultured on plastic, confirming differential gene expression and increased proliferation in I148M *vs.* PNPLA3-WT HSCs (Fig. S1). Most pathways modulated by the *PNPLA3* variant were related to mitochondria metabolism and oxidative stress (increased "Oxidative Phosphorylation" and "NRF2-mediated oxidative stress response") or to glucose and lipid metabolism (increased "Apeline adipocyte signalling pathway" and decreased "PPARα/RXRα activation") along with ECM remodelling (increased "ILK signalling") (Fig. 1B). Increased fibrogenesis, synthesis of lipids and reduction of hydrogen peroxide in PNPLA3-I148M HSCs was also identified by Biofunctions analysis (Fig. 1C). Analysis of the activation status of the network of modulators which might drive pathway dysregulation (upstream regulator analysis) predicted a strong activation of inflammatory and proliferative genes, but also many activators linked to oxidative stress, lipid metabolism and an extended number of intracellular mediators of transforming growth factor-β1 (TGFB1) signalling (Fig. 1A). In addition, transcriptomic analysis highlighted a group of significantly upregulated and downregulated target genes (Fig. 1D).

Before proceeding to target validation, a second round of analysis was performed to select pathways and genes modulated by the *PNPLA3* variant in HSCs and potentially relevant for NAFLD progression. This was achieved by combining transcriptomic data on primary HSCs isolated from different donors (*in vitro*) with transcriptomic data obtained from patients' biopsies (*Human*) where the *PNPLA3* variant had previously been identified as a major driver of NAFLD disease severity and gene expression variability.[38] Comparisons highlighted a large pool of significantly modulated genes shared between the two datasets (Fig. 1E). The selection of shared pathways and biofunctions was made by choosing pathways significantly enriched and modulated in the same direction (Z-score >0 or Z-score <0) in both the datasets. This analysis confirmed that the presence of the *PNPLA3* variant is associated with the modulation of a large set of pathways related to mitochondria/oxidative stress (increased "NRF2-mediated oxidative stress response"), glucose/lipid metabolism (decreased "Glucose metabolism disorder") and ECM signalling (increased "Hepatic Fibrosis", "ILK Signalling") (Fig. 1F,H). Upstream regulator analysis showed a similar trend to the *in vitro* analysis, with a large set of activated modulators related to ECM signalling and TGFB1 having one of the highest activation Z-scores (Fig. 1G). The analysis predicted TGFB1 to be a major upstream regulator of half of the deregulated canonical pathways and most of the target genes identified by transcriptomics (Fig. 1F,I, pathways/genes marked by a red asterisk, Table S3, Fig. S8). Overall, these data suggest an impact of the *PNPLA3* I148M variant on the fibrogenic phenotype of HSCs with an involvement of mitochondria/lipid metabolism and oxidative stress, with TGFB1 playing a key role. Importantly, these mechanisms seem to be specific to HSCs, as previously published data on the same liver biopsy dataset[38] identified pathways and target genes related to inflammation and cancer development as majorly dysregulated, which are not significantly affected in the RNA sequencing dataset of primary HSCs (Table S4). Preliminary gene expression investigations (Fig. S2) and literature study prompted us to focus on NR4A1 (also known as NUR77), an antifibrotic target of TGFB1, which can also be modulated by the antioxidant-related transcription factors JUN and FOS (Fig. 1J).

The 3D HSC model recapitulates *PNPLA3* I148M-induced modulation of intracellular pathways observed in human livers and 2D models

Findings from transcriptomic data were validated using an established 3D ECM scaffold model.[35,36] The healthy and cirrhotic liver microenvironment was recapitulated by using acellular scaffolds obtained from healthy and cirrhotic human livers which were repopulated with patient-isolated PNPLA3-WT or PNPLA3-I148M HSCs and challenged with chronic TGFB1 treatment (Fig. S3A). Gene expression analysis on PNPLA3-WT or PNPLA3-I148M HSCs cultured on healthy and cirrhotic 3D scaffolds was performed using Nanostring™ Technologies' nCounter® Human Fibrosis 700 genes panel (Fig. 2A). Gene set analysis highlighted pathways driving differential expression between PNPLA3-WT and -I148M HSCs and cultured on healthy or cirrhotic ECM scaffolds. The top 30 pathways driving differential expression in WT *vs*. PNPLA3-I148M HSCs were related to "Collagen or ECM Biosynthesis and modification" and "Hippo Pathway" (upregulation of

protein expression. (D,E) *TGFB1* and *SERPINE1* gene expression. (F,G) COL1A1 protein expression. Blots from WT and PNPLA3-I148M HSCs or healthy and cirrhotic scaffolds were processed in parallel. (H) Pro-COL1A1 protein secretion. (I) *BMP1* gene expression; (*****p* <0.001/****p* <0.005/***p* <0.01/**p* <0.05; n = 1 donor per each genotype and n = 3/4/6 biological replicates per each condition (protein expression/gene expression/protein secretion); data analysed via three-way ANOVA with Tukey's multiple comparison test). ECM, extracellular matrix; GSA, gene set analysis; HSCs, hepatic stellate cells; WT, wild-type.

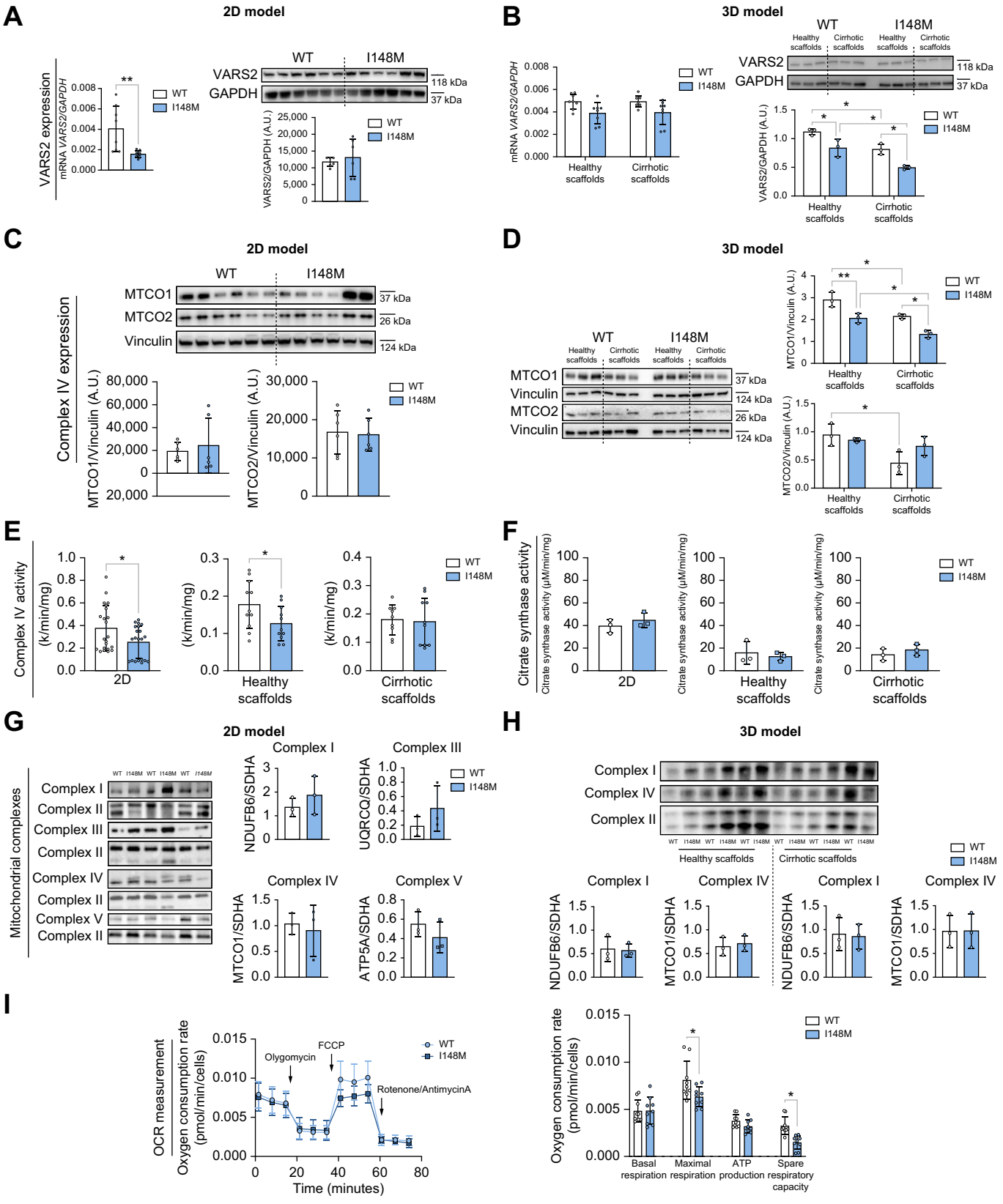

Fig. 3. PNPLA3-I148M HSCs have impaired mitochondrial function compared to PNPLA3-WT HSCs. Analysis of expression of genes and proteins in PNPLA3-I148M *vs.* WT HSCs. (A,B) VARS2 gene and protein expression in HSCs cultured (A) in 2D for 3 days or (B) in healthy or cirrhotic scaffolds for 14 days. (C,D) Protein expression of complex IV mitochondrially encoded subunits MTCO1 and MTCO2 in HSCs cultured (C) in 2D for 3 days or (D) in healthy or cirrhotic scaffolds for 14 days. (E,F) Complex IV and citrate synthase activity in HSCs cultured in 2D, healthy or cirrhotic scaffolds for 3 or 14 days. (G,H) Quantification of mitochondrial respiratory chain complexes using BN-PAGE in HSCs cultured (G) in 2D for 3 days or (H) on healthy or cirrhotic scaffolds for 14 days; SDHA (Complex II) was used as loading

thrombospondins and integrins with downregulation of MMPs), "TGFB1 signalling" (increasing F11R and SERPINE1), lipid metabolism ("PPAR Signalling", "De novo lipogenesis" and "Fatty Acid metabolism") and "Oxidative stress". When comparing HSC cultures in 3D cirrhotic ECM *vs*. 3D healthy ECM, the top 30 impacted pathways showed differential expression of genes related to "Gluconeogenesis", "Oxidative Stress", "Hippo Pathways" but also TGFB1 and PDGF signalling (Fig. 2A).

Next, the TGFB1 signalling pathway was analysed: in PNPLA3-I148M HSCs and in cells cultured on the 3D cirrhotic ECM, TGFB1 protein expression was significantly upregulated (Fig. 2B,C), while latent TGFB1 secretion was significantly upregulated by 3D cirrhotic ECM in PNPLA3-WT HSCs (Fig. S3B). Furthermore, in line with TGFB1 upregulation, PNPLA3-I148M HSCs showed a pro-fibrotic behaviour which was demonstrated by the upregulation of SERPINE1 (Fig. 2E), involved in ECM accumulation,[39,41] bone morphogenic protein 1 (Fig. 2I), the enzyme cleaving the C-terminal of pro-collagen 1a1 to mature COL1A1, and COL1A1 protein expression (Fig. 2F,G) and pro-COL1A1 protein secretion (Fig. 2H).

Overall, the pathways that appeared to be modulated in the 3D model were similar to those highlighted by the RNA sequencing data. In particular, TGFB1 – highlighted by transcriptomic data as a key activated upstream regulator – showed increased signalling in PNPLA3-I148M HSCs *vs*. PNPLA3-WT HSCs and in cirrhotic scaffolds compared to healthy scaffolds. Hence, the 3D model, which can recapitulate the changes identified by the RNA sequencing data, was chosen for further investigation.

The *PNPLA3* I48M variant causes mitochondrial dysfunction in HSCs

In vitro transcriptomic analysis highlighted a dysregulation of many mitochondrial metabolism-related pathways, including the mitochondrial enzyme valyl-tRNA synthetase 2 (VARS2), which was downregulated in PNPLA3-I148M HSCs. This was confirmed at the gene expression level in HSCs cultured in 2D with no changes at the protein expression level (Fig. 3A). When HSCs were cultured on 3D ECM scaffolds, the same trend of decreased *VARS2* gene expression in PNPLA3-I148M HSCs was observed, with an additional significant decrease of VARS2 protein content observed when both WT and PNPLA3-I148M HSCs were cultured on cirrhotic scaffolds compared to healthy scaffolds (Fig. 3B). VARS2 is a key enzyme in the synthesis of the mitochondrial DNA-encoded subunits of the respiratory chain enzyme complexes.[42] Hence, the abundance of two of the 13 mitochondrial DNA-encoded subunits and the five mitochondrial respiratory chain complexes (complexes I–V) was measured in WT and PNPLA3-I148M HSCs cultured in 2D or 3D scaffolds. The two mitochondrially encoded subunits of complex IV, mitochondrially encoded cytochrome C oxidase I/II (MTCO1/MTCO2), were significantly downregulated in cells carrying the *PNPLA3* I148M variant, with MTCO1 content also being lower in the presence of the 3D cirrhotic ECM compared to healthy ECM, while no significant difference was observed in cells cultured in 2D (Fig. 3C,D). Complex IV enzymatic activity was also lower in PNPLA3-I148M *vs.* WT HSCs cultured in 2D or 3D healthy scaffolds, but not in cirrhotic scaffolds (Fig. 3E). In contrast, the expression of the other mitochondrial respiratory chain complexes, resolved on blue native gels, was not significantly affected by the *PNPLA3* I148M variant or 3D cirrhotic ECM (Fig. 3G,H). Furthermore, mitochondrial respiratory activity, which was quantified by measuring the oxygen consumption rate, was decreased in PNPLA3-I148M *vs.* WT HSCs. Specifically, while basal respiration was equal regardless of the presence of the *PNPLA3* I148M mutation, maximal respiration observed in stress conditions (FCCP injection) was lower in PNPLA3-I148M HSCs compared to WT (Fig. 3I). These results suggest a *PNPLA3*-I148M-driven mitochondrial dysfunction in HSCs, not due to a lower mitochondrial number supported by unchanged activity of the citrate enzyme system (Fig. 3F), but rather to a deficiency in complex IV expression and activity (Fig. 3E).

Mitochondrial dysfunction and VARS2 depletion have both been linked to activation of the integrated stress response (ISR).[43,44] Analysis on the RNA sequencing conducted on liver biopsies highlighted a large pool of deregulated genes linked to ISR. Nevertheless, the RNA sequencing dataset and the expression of important ISR genes in the HSCs cultured on liver scaffolds did not provide conclusive evidence of whether the ISR pathway might be activated in HSCs due to the presence of the PNPLA3 mutation (Table S5, Fig. S5). Hence, we next focused on how mitochondrial dysfunction might affect the antioxidant capacity of PNPLA3-I148M HSCs.

Antioxidant response is reduced in PNPLA3-I148M HSCs

In the presence of mitochondrial dysfunction, inefficient nutrient oxidation leads to a low ratio of ATP production/oxygen consumption. This can lead to an increased production of superoxide anions and consequent oxidative stress, which is known to play a key role in the progression of fatty liver disease.[45] Given the identification by Ingenuity Pathway Analysis of several oxidative stress-related pathways which were dysregulated by the *PNPLA3* I148M variant, and the mitochondrial dysfunction observed in the 3D model of HSCs, we further investigated the antioxidant capacity of the cells. Thus, HSCs grown in the 3D model of healthy and cirrhotic ECM were exposed to TGFB1, known to be involved in oxidative stress processes[46] and identified as a key upstream regulator of gene expression variability in PNPLA3-I148M HSCs by NGS. Gene expression of cytoglobin B (CYGB), an oxygen transporter, was significantly decreased in HSCs carrying the *PNPLA3* I148M variant or by TGFB1 treatment in healthy scaffolds. Gene expression of nuclear factor erythroid 2-related factor 2 (*NRF2*), a key antioxidant enzyme, followed a similar pattern and its

control. (l) Seahorse analysis showing the OCR in HSCs. (**p <0.01/*p <0.05, Gene expression: n = 2 donors per genotype, n = 4 biological replicates per condition; Protein expression: n = 3 (2D) or 1 (3D) donors per genotype, n = 3 biological replicates per condition; Enzymatic activity: n = 4 donors per genotype, n = 4/5 biological replicates per condition; BN-PAGE: n = 3 donors per genotype, n = 1 biological replicate per condition; Seahorse: n = 3 donors per genotype, n = 3 biological replicates; data analysed via Student's *t* test or two-way ANOVA with Tukey's multiple comparison test). HSCs, hepatic stellate cells; OCR, oxygen consumption rate; WT, wild-type.

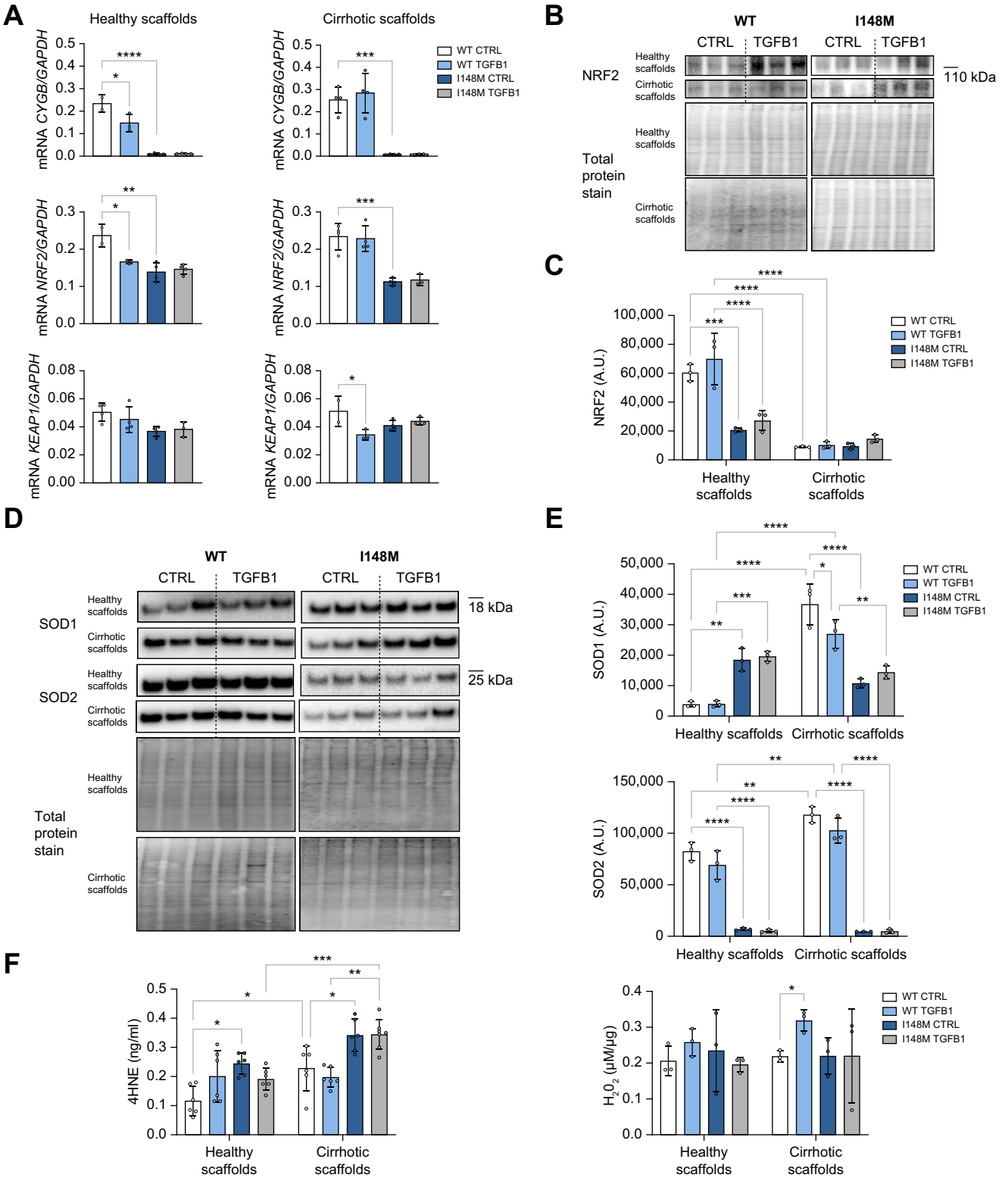

Fig. 4. Characterization of antioxidant response of PNPLA3-I148M or WT HSCs cultured in healthy or cirrhotic scaffolds. Analysis of expression of genes and proteins in PNPLA3-I148M *vs.* WT HSCs cultured on healthy or cirrhotic scaffolds with or without TGFB1 (5 ng/ml). (A) Gene expression analysis of *CYGB, NRF2, KEAP1*; (B,C,D,E) NRF2, SOD1, SOD2 protein expression. Blots from WT and PNPLA3-I148M HSCs or healthy and cirrhotic scaffolds were processed in parallel. (F) Quantification of secreted H_20_2 and 4-HNE; (****p <0.001/***p <0.005/**p <0.01/*p <0.05, n = 1 donor per genotype, n = 3/4/6 biological replicates per condition (protein expression/gene expression/protein secretion); data analysed via two- or three-way ANOVA with Tukey's multiple comparison test). 4-HNE, 4-hydroxynonenal; HSCs, hepatic stellate cells; WT, wild-type.

repressor, *KEAP1* (kelch like ECH associated protein 1), was downregulated following TGFB1 treatment in PNPLA3-I148M *vs.* WT cells in the presence of the cirrhotic ECM (Fig. 4A). These results were further confirmed by protein expression analysis showing a decrease of NRF2 in the presence of the *PNPLA3* I148M variant and in the 3D cirrhotic ECM (Fig. 4B,C). Interestingly, the amount of superoxide dismutase (SOD)2, the mitochondrial-specific superoxide dismutase, was decreased in PNPLA3-I148M *vs.* WT HSCs, whereas the same pattern was not observed for the cytoplasmic superoxide dismutase SOD1 (Fig. 4D,E). In addition, measurement of ROS release showed a significant increase in the amount of lipid peroxidation products such as 4-hydroxynonenal (4-HNE), driven by the presence of the *PNPLA3* I148M variant and further increased by the 3D cirrhotic ECM. A similar pattern was not observed in the release of other endogenous ROS such as H_2O_2, although this was increased by TGFB1 treatment in cirrhotic scaffolds (Fig. 4F). These data indicate an impaired antioxidant response in PNPLA3-I148M HSCs, which leads to an increase in ROS. Importantly, this effect is significantly enhanced in the presence of the cirrhotic ECM or after exposure to TGFB1 and supports the findings from the transcriptomic data.

Antifibrotic NR4A1 is downregulated in PNPLA3-I148M *vs.* WT HSCs

NR4A1 is a transcription factor of the nuclear receptors superfamily that governs multiple cell functions including metabolism,[47,48] oxidative stress and multiple aspects of wound-healing.[49] NR4A1 is also described as an endogenous antifibrotic gene modulated by TGFB1, *i.e.* upon chronic TGFB1-induced NR4A1 phosphorylation, the NR4A1 protein translocates from the nucleus to the cytoplasm, becoming inactive and unable to counteract the pro-fibrogenic effect of TGFB1.[50] NR4A1 was highlighted by NGS as differentially modulated in the *PNPLA3* I148M variant. *NR4A1* gene expression was decreased following chronic TGFB1 treatment only in HSCs grown in cirrhotic scaffolds (Fig. 5A). In addition, the total amount of NR4A1 protein was strikingly lower in PNPLA3-I148M *vs.* WT HSCs, whereas the phosphorylated fraction of NR4A1 was higher in PNPLA3-I148M *vs.* WT HSCs and further increased by chronic treatment with TGFB1 when cells were cultured in the 3D cirrhotic scaffold (Fig. 5B,C). Importantly, inactivation of NR4A1 in PNPLA3-I148M HSCs was confirmed by the downregulation of gene expression of NR4A1 targets as analysed by Nanostring™ nCounter® for Human Fibrosis and shown in Fig. 5D. Furthermore, phosphorylation (/inactivation) of NR4A1 is linked to its cytoplasmic localization.[50,51] Accordingly, immunohistochemistry of NR4A1 and phospho-NR4A1 confirmed the localization of the active NR4A1 mainly in the cellular nuclei and of the inactive phosphorylated NR4A1 mainly in the cytoplasm in both WT (Fig. 5E) and PNPLA3-148M HSCs (Fig. 5F).

NR4A1 agonist Csn-B increases NR4A1 only in HSCs cultured in 3D healthy scaffolds

To further explore whether an increase in NR4A1 affects the mitochondrial/antioxidant/pro-fibrogenic features of HSCs, and whether this process can be modulated by *PNPLA3* genotype, HSCs exposed to TGFB1 were supplemented with the NR4A1 natural agonist cytosporone B (Csn-B).[52] The dosage of Csn-B was determined using a dose-response curve of increasing Csn-B concentrations which were tested on both WT and PNPLA3-I148M HSCs cultured in 2D and in the 3D healthy scaffold. Csn-B was toxic for cells cultured in 2D only at the highest concentration (20 μM), while in the 3D model, toxicity of Csn-B was detectable at 10 μM (Fig. 6A). Therefore, 1 μM and 5 μM were chosen as low and high concentrations of Csn-B for the following experiments. First, a single 24-hour treatment with Csn-B led to an increase in NR4A1 and a decrease of phospho-NR4A1 in both WT and PNPLA3-I148M HSCs cultured in healthy scaffolds (Fig. S6). Therefore, the next experiments were performed in the presence of both chronic TGFB1 and Csn-B treatment (48 h*3). Gene expression analysis showed a Csn-B-dependent upregulation of NR4A1 only in PNPLA3-WT HSCs grown in healthy scaffolds (Fig. 6B), while total NR4A1 protein was significantly increased by Csn-B (1 μM) only in PNPLA3-I148M HSCs cultured on healthy scaffolds. Interestingly, the phosphorylated fraction of NR4A1 was decreased by Csn-B (1 μM) in both WT and PNPLA3-I148M HSCs, but only when the cells were cultured in healthy scaffolds (Fig. 6C,D).

Csn-B attenuates TGFB1-induced production of COL1A1 and increases antioxidant enzymes in both WT and PNPLA3-I148M HSCs

Treatment with Csn-B (at both 1 μM and 5 μM) decreased COL1A1 protein expression in both WT and PNPLA3-I148M HSCs cultured in healthy and cirrhotic scaffolds (Fig. 7A,B). TGFB1 protein expression was also downregulated by Csn-B in PNPLA3-WT HSCs, whereas the effect was not significant in PNPLA3-I148M HSCs or cirrhotic scaffolds (Fig. 7C,D). Furthermore, secretion of Pro-Col1a1 followed a similar trend when both WT and PNPLA3-I148M HSCs were cultured in healthy scaffolds but without reaching statistical significance (Fig. 7E). Importantly, treatment with Csn-B also increased NFR2 and CYGB gene and protein expression in PNPLA3-I148M HSCs cultured in healthy scaffolds, with a similar trend observed in PNPLA3-WT HSCs (Fig. 7F,G). Therefore, a Csn-B-induced increase of total active NR4A1 with a consequent decrease of the inactivated phospho-NR4A1 in HSCs resulted in the downregulation of pro-fibrogenic markers, with a stronger effect in PNPLA3-WT HSCs, and an increase in antioxidant enzymes in PNPLA3-I148M HSCs. Importantly, this effect was not associated with significant differences when the cells were cultured in the 3D cirrhotic ECM, clearly indicating an ECM-specific effect.

Notably, our results also show that regulation of the translational machinery might be driven by different pathways in PNPLA3-I148M compared to PNPLA3-WT HSCs. In fact, post-translational modification of NR4A1 can be mediated by Akt, Erk or other MAPK kinases in different chronic conditions.[50,51,53] Indeed, in PNPLA3-WT HSCs, TGFB1 increased the phosphorylated form of Akt, and when combined with Csn-B, this effect was abrogated, suggesting a consequent Akt-driven phosphorylation of NR4A1. This effect was not observed in PNPLA3-I148M HSCs (Fig. S7). In contrast, TGFB1 increased the phosphorylated form of Erk, and this effect was abrogated when combined with Csn-B, in PNPLA3-I148M but not PNPLA3-WT HSCs (Fig. S7). Therefore, this suggests a different mechanism of phosphorylation of NR4A1, which is driven by Akt in PNPLA3-WT HSCs but by Erk in PNPLA3-I148M HSCs.

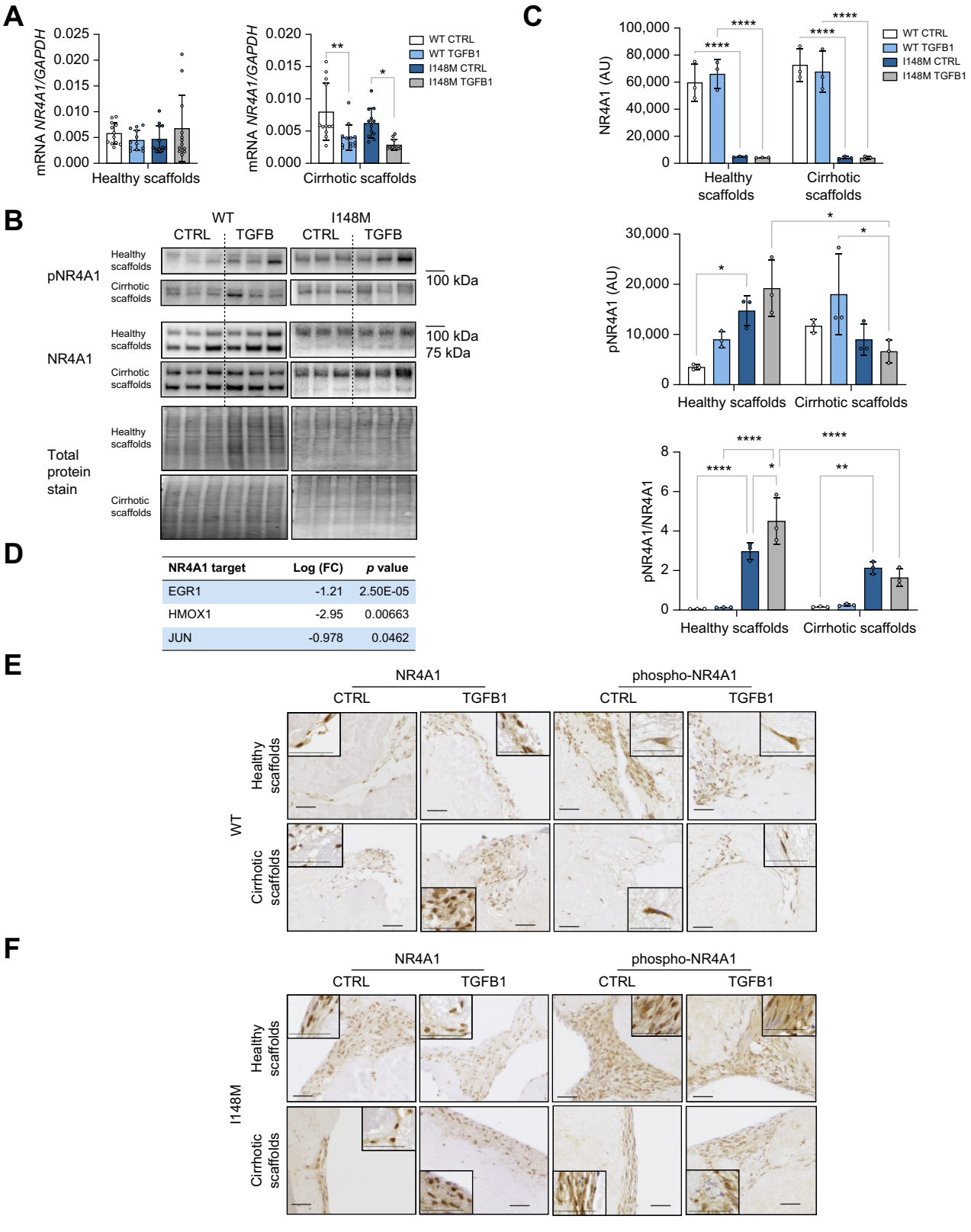

Fig. 5. NR4A1 expression and TGFB1 regulation in PNPLA3-WT or PNPLA3-I148M-genotyped HSCs. Analysis of expression of genes and proteins in PNPLA3-I148M *vs.* WT HSCs cultured on healthy or cirrhotic scaffolds with or without TGFB1 (5 ng/ml). (A) Gene expression of NR4A1 (**p <0.01/*p <0.05, n = 3 donors per genotype, n = 4 biological replicates per condition; data analysed via two-way ANOVA with Tukey's multiple comparison test); (B,C) Protein expression of NR4A1, pNR4A1 and ratio of pNR4A1 to NR4A1. Blots from WT and PNPLA3-I148M HSCs or healthy and cirrhotic scaffolds were processed in parallel. NR4A1 was quantified as the sum of two bands (100 kDa and 75 kDa). (****p <0.001/***p <0.005/**p <0.01/*p <0.05, n = 1 donor per genotype, n = 3 biological replicates per condition; data analysed via three-way ANOVA with Tukey's multiple comparison test); (D) Gene expression fold change of NR4A1 target genes in I148M-PNPAL3 HSCs *vs.* PNPLA3-

Discussion

The *PNPLA3* I148M variant accounts for the largest fraction of inherited predisposition to the development of any progressive chronic liver disease, including evolution of cirrhosis and hepatocellular carcinoma.[16,21,54] This variant has been associated with liver fat accumulation, hepatic inflammation, and susceptibility to developing fibrosing steatohepatitis.[16] Several studies have demonstrated the association between *PNPLA3* I148M and the development and severity of liver fibrosis[20–22] and how *PNPLA3* is correlated to HSC activation.[23] Nonetheless, the mechanism(s) underlying the pro-fibrogenic effect of *PNPLA3* on human HSCs have not been clarified yet. In a previous study, transcriptomic analysis of liver biopsies was utilized to highlight the impact of the PNPLA3 I148M variant on the liver transcriptome of patients with severe NAFLD and this was correlated with an increased inflammatory signature specifically in hepatocytes.[38] In our study, comparative transcriptomic analysis of both *in vitro*-cultured HSCs and patient liver biopsies identified *PNPLA3* I148M-driven disruption of mitochondrial function and antioxidant responses in HSCs. This was accompanied by increased TGFB1 signalling which dampened the activity of TGFB1's endogenous antifibrotic inhibitor NR4A1.

Mitochondrial dysfunction is related to the development of various liver diseases[55] and has been established as one of the driving forces for the progression of NAFLD.[56] Despite the attempts of the liver to recover from fat accumulation by increasing oxidative phosphorylation in the initial phase of NAFLD, mitochondrial adaptation is insufficient to stop the progress of the disease, leading to impaired mitochondrial respiration and exhaustion of oxidative phosphorylation in NASH.[57–59] The presence of the *PNPLA3* I148M variant has been associated with a decreased mitochondrial function in Huh-7 hepatoma cells and LX2 cells.[25,60] Importantly, in this study, we showed that human primary HSCs carrying the *PNPLA3* I148M variant had a lower oxygen consumption rate compared to wild-type cells. In addition, we demonstrated a lower expression, which coincided with a lower enzyme functionality of complex IV of the mitochondrial respiratory chain contributing to this process. Complex IV was shown to be decreased both in patients with NAFLD,[61] animal models of fatty liver disease,[62] and HBV-infected cells[63] and is the most common respiratory chain complex involved in liver failure.[59] Importantly, we were able to link complex IV insufficiency to the *PNPLA3* I148M variant and thus with mitochondrial dysfunction in HSCs. Abnormal reduction of respiratory complexes promotes the production of superoxides,[64] which are associated with the progression of chronic liver disease.[65] ROS are produced in physiological conditions and are important for physiological redox signalling. Regardless, overproduction of ROS and impaired capacity of the antioxidant system leads to oxidative stress.[66] Studies have shown that loss of complex IV in brain and heart tissue causes a three-fold increase in ROS levels produced at the level of complex I by mitochondria.[67] Accordingly, we observed an increased secretion of ROS in HSCs carrying the *PNPLA3* I148M variant. The major increase was observed for secreted 4-HNE, a product of lipid peroxidation which damages the mitochondrial genome,[68,69] and can directly attack and inactivate respiratory chain components including complex IV.[70] This can lead to a vicious cycle triggering ROS generation by the respiratory chain[56] and may act as a potent pro-fibrogenic stimulus for HSCs.[71]

In addition, we also observed a decreased antioxidant capacity in PNPLA3-I148M HSCs, which showed lower levels of CYGB, NRF2 and SOD2 compared to WT cells. These data agree with patient and *in vivo* animal data on NAFLD and NASH,[72–74] as well as with the further hampering of antioxidant enzyme quantity caused by the presence of TGFB1.

As previously reported, TGFB1 modulates PNPLA3 expression in HSCs[25,75] and we demonstrated in the present study that *PNPLA3*-I148M HSCs are characterized by increased TGFB1 signalling, which is known to increase pro-fibrogenic and inflammatory features[76] as well as oxidative stress in HSCs.[46] Recently, NR4A1 was identified as an endogenous inhibitor of TGFB1 signalling in the context of chronic fibrogenesis,[50] and was reported to be enriched in HSCs in the liver (Human Protein Atlas, data available from v21.1.proteinatlas.org[77]), and proposed as a new anti-fibrogenic marker.[78–80] In the present study, the transcriptomic data suggested a dysregulation of NR4A1, which was confirmed by a marked decrease and inactivation of its protein expression in PNPLA3-I148M HSCs, coinciding with an increase in TGFB1 and COL1A1 expression. This effect was abolished by treatment with Csn-B, an agonist of NR4A1, which decreased inactive phosphorylated NR4A1, thus counteracting the pro-fibrogenic effect of TGFB1 and directly implicating NR4A1 in the mechanism by which PNPLA3-I148M promotes HSC activation. Interestingly, our data suggest that the mechanism leading to the phosphorylation of NR4A1 might be different between PNPLA3-WT and PNPLA3-I148M HSCs. In fact, Akt appeared to drive the phosphorylation of NR4A1 in PNPLA3-WT HSCs treated with TGFB1, in agreement with other studies on fibroblasts in chronic fibrotic conditions.[50] On the other hand, in HSCs carrying the PNPLA3-I148M variant, the same process appeared to be driven by Erk. This further supports the existence of different molecular mechanisms and activated pathways related to the presence of the PNPLA3 I148M variant.

Remarkably, the increase in NR4A1 activity, induced by treatment with Csn-B, was associated with an increase in the antioxidant enzyme NRF2 in PNPLA3-I148M HSCs, suggesting an inhibitory effect of NR4A1 on both the fibrogenic and oxidative stress pathways in HSCs. NR4A1 is involved in regulating oxidative stress in different conditions depending on cell type and pathological conditions investigated.[81–84] Importantly, NR4A1 expression has been found to be beneficial in mouse hepatocytes by promoting antioxidant fibroblast growth factor 21 secretion,[85] which, together with our findings in HSCs, makes it an interesting target for the treatment of fatty liver diseases.

WT HSCs cultured on ECM scaffolds (n = 2 donors per genotype, n = 3 biological replicates per ECM condition) obtained from Nanostring™ analysis; (E,F) Immunohistochemical staining of NR4A1 and phospho-NR4A1 (brown – NR4A1/phosphoNR4A1, blue/purple – chromatin, scale bar = 0.05 mm). ECM, extracellular matrix; HSCs, hepatic stellate cells; WT, wild-type.

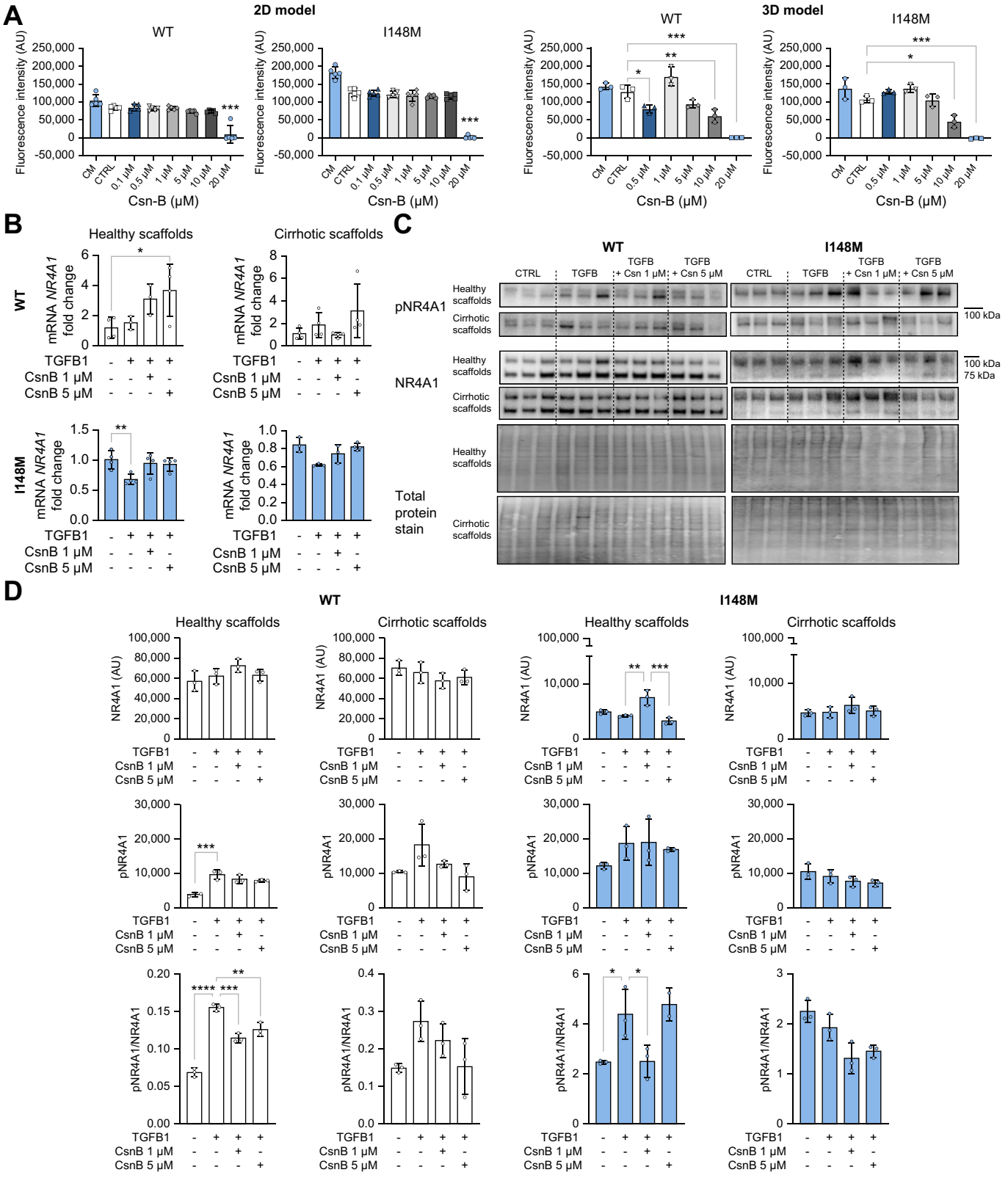

Fig. 6. Effect of the natural agonist Csn-B on NR4A1 expression in PNPLA3-WT or PNPLA3-I148M-genotyped HSCs. (A) Viability response of WT or PNPLA3-I148M HSCs cultured in 2D or 3D healthy ECM liver scaffolds to Csn-B. Cells were exposed with a dose escalation of Csn-B (2D: 0.1, 0.5, 1, 5, 10, 20 μM for 24 h, n =5 per condition; 3D: 0.5, 1, 5, 10, 20 μM for 48 h*3, n = 3 per condition, n = 1 donor per genotype; data analysed via one-way ANOVA with Tukey's multiple comparison test). Analysis of expression of genes and proteins in PNPLA3-I148M *vs.* WT HSCs cultured on healthy or cirrhotic scaffolds with TGFB1 (5 ng/ml) and Csn-B (1 μM or 5 μM). (B) Gene expression of *NR4A1*. (C,D) Protein expression of NR4A1, pNR4A1 and ratio of pNR4A1 to NR4A1. Blots from WT and PNPLA3-I148M HSCs or healthy and cirrhotic scaffolds were processed in parallel. NR4A1 was quantified as the sum of two bands (100 kDa and 75 kDa). (*****p* <0.001/****p* <0.005/***p* <0.01/**p* <0.05, n = 1 donor per genotype, n = 4/3 biological replicates per condition (gene expression/protein expression); data analysed via one-way ANOVA with Tukey's multiple comparison test). Csn-B, cytosporone B; ECM, extracellular matrix; HSCs, hepatic stellate cells; WT, wild-type.

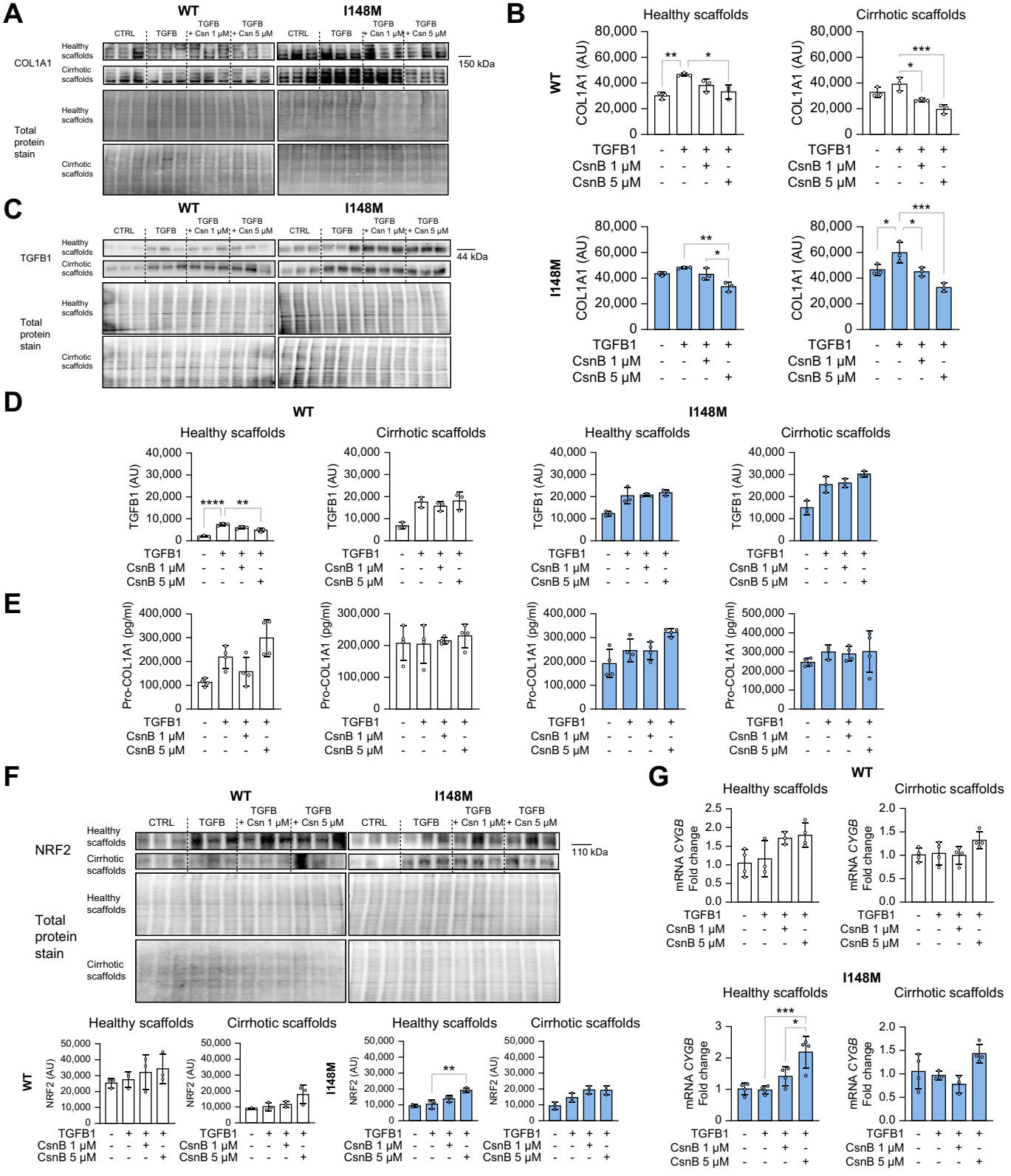

Fig. 7. Effect of the natural agonist Csn-B on activation markers and antioxidant enzymes in PNPLA3-WT or PNPLA3-I148M-genotyped HSCs. Analysis of expression of genes and proteins in PNPLA3-I148M *vs.* WT HSCs cultured on healthy or cirrhotic scaffolds with TGFB1 (5 ng/ml) and Csn-B (1 μM or 5 μM). (A-D) Protein expression of (A,B) COL1A1 and (C,D) TGFB1. Blots from WT and PNPLA3-I148M HSCs or healthy and cirrhotic scaffolds were processed in parallel. (E) Protein secretion of Pro-COL1A1. (F) Protein expression of NRF2. Blots from WT and PNPLA3-I148M HSCs or healthy and cirrhotic scaffolds were processed in parallel. (G) Gene expression of *CYGB*; (****p* <0.005/***p* <0.01/**p* <0.05, n = 1 donor per genotype, n = 3/4 biological replicates per condition (protein expression/gene expression and protein secretion); data analysed via one-way ANOVA with Tukey's multiple comparison test). Csn-B, cytosporone B; HSCs, hepatic stellate cells; WT, wild-type.

It is important to note the differential responses of both PNPLA3-WT and I148M HSCs when cultured on 3D cirrhotic *vs.* healthy ECM. More specifically, one should note the imbalance of oxidative stress *vs.* antioxidant enzyme expression, the increased TGFB1 and COL1A1 expression, and the decreased NR4A1 content together with the inability of Csn-B to increase NR4A1 expression when HSCs were cultured on the 3D cirrhotic scaffolds. These effects can be attributed to the differences in ECM protein composition,[36] 3D-architecture, and physico-chemical properties,[35] as previously shown by our group.[34] Overall, our study indicates the need for a complex 3D model which includes the presence and tissue architecture of the healthy, and human cirrhotic ECM that can provide much more information compared to cell culture on plastic or 3D models devoid of normal or pathological human-derived liver ECM. In this study we did not determine the effect of co-culturing primary HSCs with other single nucleotide polymorphism-genotyped hepatic cell types; however, we previously demonstrated the effect of the PNPLA3 variant in single and co-cultures of LX2 and HepG2 cells bioengineered in healthy and cirrhotic 3D scaffolds in the context of pro-fibrogenic and anti-cancer treatment by using first-and second-line drugs and identified two different drug-induced mechanisms depending on the 3D ECM microenvironment.[37] In the present study we further deconvoluted the role of primary human HSCs carrying the PNPLA3 variant *vs.* PNPLA3-WT and their cell behaviour in this innovative 3D platform. One further limitation of this study lies in the fact that no *in vivo* model was used. Although genetically modified mouse models carrying the PNPLA3 I148M variant have shown hepatic fat accumulation,[27–29] variations occur depending on the *in vivo* model used, the type of diet, the time points investigated,[86,87] as well as gender variation[88] which further highlights the extent of the impact of PNPLA3 on fatty liver disease.

In summary, our study demonstrates the impact of the *PNPLA3* I148M variant on HSC pathways deregulation, linking it for the first time in detail with mitochondrial and antioxidant dysfunction. This was achieved by transcriptomic analysis of an *in vitro* HSC model and patients' samples followed by validation of findings in a complex 3D model of human-derived liver decellularized scaffolds recapitulating the healthy and cirrhotic liver microenvironment. Furthermore, our study highlights the importance of TGFB1 and its endogenous inhibitor NR4A1 in HSC fibrogenesis and in the context of the *PNPLA3* variant, with NR4A1 being a potential antifibrotic drug target for the treatment of chronic liver diseases.

Affiliations

[1]*Regenerative Medicine and Fibrosis Group, Institute for Liver and Digestive Health, University College London, Royal Free Campus, London, UK;* [2]*Research Department of Surgical Biotechnology, Division of Surgery and Interventional Science, University College London, London, UK;* [3]*Department of Clinical and Movement Neurosciences, UCL Queen Square Institute of Neurology, University College London, London UK;* [4]*Laboratory of Hepatic Metabolism and NAFLD, Roger Williams Institute of Hepatology, London, UK;* [5]*Clinica Medica "Frugoni", Interdisciplinary Department of Medicine, University of Bari "Aldo Moro", Bari, Italy;* [6]*Department of Pathophysiology and Transplantation, Università degli Studi di Milano, Milan, Italy;* [7]*Sheila Sherlock Liver Centre, Royal Free London NHS Foundation Trust, London, UK;* [8]*Precision Medicine, Biological Resource Center, Fondazione IRCCS Ca' Granda Ospedale Maggiore Policlinico, Milan, Italy;* [9]*Department of Molecular and Clinical Medicine, Institute of Medicine, Sahlgrenska Academy, Wallenberg Laboratory, University of Gothenburg, Gothenburg, Sweden;* [10]*Department of Cellular Pathology, Royal Free London NHS Foundation Trust, London, UK*

Abbreviations

4-HNE, 4-hydroxynonenal; ALD, alcohol-related liver disease; CLD, chronic liver disease; COL1A1, collagen type I alpha 1 chain; Csn-B, cytosporone B; CYGB, cytoglobin B; ECM, extracellular matrix; HSCs, hepatic stellate cells; ISR, integrated stress response; MTCO1/MTCO2, mitochondrially encoded cytochrome C oxidase I/II; NAFLD, non-alcoholic fatty liver disease; NASH, non-alcoholic steatohepatitis; NGS, next-generation sequencing; NRF2, nuclear factor erythroid 2-related factor 2; PNPLA3, patatin-like phospholipase domain-containing 3; ROS, reactive oxygen species; SOD1/SOD2, superoxide dismutase 1/2; TGFB1, tumor growth factor-β1; VARS2, valyl-tRNA synthetase 2; WT, wild-type.

Financial support

MV is supported by the Foundation of Liver Research (Intramural) and AIRC (IG2022 Grant n. 27521). This research was funded by a Juan Rodés PhD Student Fellowship of the European Association for the Study of the Liver-EASL (Elisabetta Caon) and by the UCL NIHR Biomedical Research Centre BRC648.III.KR.101350 (Krista Rombouts).

Conflict of interest

Giuseppe Mazza, Walid Al-Akkad and Massimo Pinzani are patent holders of the decellularization protocol. Maria Giovanna Vilia and Giuseppe Mazza are full time employees at Engitix Therapeutics Ltd. Walid Al-Akkad, Maria Giovanna Vilia, Massimo Pinzani, Krista Rombouts and Giuseppe Mazza own shares or received stock options in Engitix Therapeutics Ltd. Andrew Hall, Tu Vinh Luong, Massimo Pinzani and Krista Rombouts receive consultancies from Engitix Therapeutics Ltd.

Please refer to the accompanying ICMJE disclosure forms for further details.

Authors' contributions

Study conceptualization and design: K.R. and E.C. Methodology: E.C., M.G.V., W.A.A., J.A.H., A.R., H., J.W.T. Analysis and interpretation of data: E.C., M.V., J.W.T., T.V.L, K.R. Acquisition of data: E.C., M.M., H.H., L.B., A.L., K.T., G.B., T.V.L. Drafting of the manuscript: E.C., K.R. Critical revision of the manuscript: J.W.T, L.V., M.V., S.R., G.M., M.P. Funding: E.C., K.R.

Data availability statement

RNAsequencing data and Nanostring nCounter data have been deposited in UCL Research Repository (UCL FigShare) and can be accessed at https://doi.org/10.5522/04/22940153.v1.

Acknowledgments

We remember Dr Elisabetta Caon who sadly passed away during the resubmission of her manuscript. We acknowledge Prof Brian Davidson, Prof Barry Fuller and Dr Amir Gander (Tissue Access for Patient Benefit) and the NHSBT, for providing tissue samples for our research. We thank Dr Luisa Ronzoni (Fondazione IRCCS Cà Granda Ospedale Maggiore Policlinico) for the selection and retrieval of human liver tissue samples. We would also like to thank UCL Genomics for performing the RNA sequencing of the primary human hepatic stellate cells used in this study.

Supplementary data

Supplementary data to this article can be found online at https://doi.org/10.1016/j.jhep.2024.01.032.

References

Author names in bold designate shared co-first authorship

[1] Cheemerla S, Balakrishnan M. Global epidemiology of chronic liver disease. Clin Liver Dis (Hoboken) 2021;17:365–370.

[2] Eslam M, Newsome PN, Sarin SK, et al. A new definition for metabolic dysfunction-associated fatty liver disease: an international expert consensus statement. J Hepatol 2020;73:202–209.

[3] Younossi Z, Tacke F, Arrese M, et al. Global perspectives on nonalcoholic fatty liver disease and nonalcoholic steatohepatitis. Hepatology 2019;69:2672–2682.
[4] Loomba R, Adams LA. The 20% rule of NASH progression: the natural history of advanced fibrosis and cirrhosis caused by NASH. Hepatology 2019;70:1885–1888.
[5] Taylor RS, Taylor RJ, Bayliss S, et al. Association between fibrosis stage and outcomes of patients with nonalcoholic fatty liver disease: a systematic Review and meta-analysis. Gastroenterology 2020;158:1611–1625 e1612.
[6] Friedman SL, Pinzani M. Hepatic fibrosis 2022: unmet needs and a blueprint for the future. Hepatology 2022;75:473–488.
[7] Pinzani M. When research on liver fibrosis made the right turn. Nat Rev Gastroenterol Hepatol 2023;20:632.
[8] Parola M, Pinzani M. Liver fibrosis: pathophysiology, pathogenetic targets and clinical issues. Mol Aspects Med 2019;65:37–55.
[9] Bottcher K, Pinzani M. Pathophysiology of liver fibrosis and the methodological barriers to the development of anti-fibrogenic agents. Adv Drug Deliv Rev 2017;121:3–8.
[10] Luedde T, Kaplowitz N, Schwabe RF. Cell death and cell death responses in liver disease: mechanisms and clinical relevance. Gastroenterology 2014;147:765–783 e764.
[11] Canbay A, Taimr P, Torok N, et al. Apoptotic body engulfment by a human stellate cell line is profibrogenic. Lab Invest 2003;83:655–663.
[12] Canbay A, Friedman S, Gores GJ. Apoptosis: the nexus of liver injury and fibrosis. Hepatology 2004;39:273–278.
[13] Rockey DC. Hepatic fibrosis, stellate cells, and portal hypertension. Clin Liver Dis 2006;10:459–479 [vii-viii].
[14] Trepo E, Valenti L. Update on NAFLD genetics: from new variants to the clinic. J Hepatol 2020;72:1196–1209.
[15] **Bianco C**, **Jamialahmadi O**, **Pelusi S**, et al. Non-invasive stratification of hepatocellular carcinoma risk in non-alcoholic fatty liver using polygenic risk scores. J Hepatol 2021;74:775–782.
[16] Romeo S, Kozlitina J, Xing C, et al. Genetic variation in PNPLA3 confers susceptibility to nonalcoholic fatty liver disease. Nat Genet 2008;40:1461–1465.
[17] He S, McPhaul C, Li JZ, et al. A sequence variation (I148M) in PNPLA3 associated with nonalcoholic fatty liver disease disrupts triglyceride hydrolysis. J Biol Chem 2010;285:6706–6715.
[18] **Pingitore P**, **Pirazzi C**, Mancina RM, et al. Recombinant PNPLA3 protein shows triglyceride hydrolase activity and its I148M mutation results in loss of function. Biochim Biophys Acta 2014;1841:574–580.
[19] **Pirazzi C**, **Valenti L**, **Motta BM**, et al. PNPLA3 has retinyl-palmitate lipase activity in human hepatic stellate cells. Hum Mol Genet 2014;23:4077–4085.
[20] Valenti L, Al-Serri A, Daly AK, et al. Homozygosity for the patatin-like phospholipase-3/adiponutrin I148M polymorphism influences liver fibrosis in patients with nonalcoholic fatty liver disease. Hepatology 2010;51:1209–1217.
[21] **Buch S**, **Stickel F**, Trepo E, et al. A genome-wide association study confirms PNPLA3 and identifies TM6SF2 and MBOAT7 as risk loci for alcohol-related cirrhosis. Nat Genet 2015;47:1443–1448.
[22] Valenti L, Dongiovanni P, Ginanni Corradini S, et al. PNPLA3 I148M variant and hepatocellular carcinoma: a common genetic variant for a rare disease. Dig Liver Dis 2013;45:619–624.
[23] Bruschi FV, Claudel T, Tardelli M, et al. The PNPLA3 I148M variant modulates the fibrogenic phenotype of human hepatic stellate cells. Hepatology 2017;65:1875–1890.
[24] Kostrzewski T, Maraver P, Ouro-Gnao L, et al. A microphysiological system for studying nonalcoholic steatohepatitis. Hepatol Commun 2020;4:77–91.
[25] Bruschi FV, Tardelli M, Einwallner E, et al. PNPLA3 I148M up-regulates hedgehog and Yap signaling in human hepatic stellate cells. Int J Mol Sci 2020:21.
[26] Bruschi FV, Claudel T, Tardelli M, et al. PNPLA3 I148M variant impairs liver X receptor signaling and cholesterol homeostasis in human hepatic stellate cells. Hepatol Commun 2019;3:1191–1204.
[27] Smagris E, BasuRay S, Li J, et al. Pnpla3I148M knockin mice accumulate PNPLA3 on lipid droplets and develop hepatic steatosis. Hepatology 2015;61:108–118.
[28] Li JZ, Huang Y, Karaman R, et al. Chronic overexpression of PNPLA3I148M in mouse liver causes hepatic steatosis. J Clin Invest 2012;122:4130–4144.
[29] Linden D, Ahnmark A, Pingitore P, et al. Pnpla3 silencing with antisense oligonucleotides ameliorates nonalcoholic steatohepatitis and fibrosis in Pnpla3 I148M knock-in mice. Mol Metab 2019;22:49–61.
[30] Lake AC, Sun Y, Li JL, et al. Expression, regulation, and triglyceride hydrolase activity of Adiponutrin family members. J Lipid Res 2005;46:2477–2487.
[31] Huang Y, He S, Li JZ, et al. A feed-forward loop amplifies nutritional regulation of PNPLA3. Proc Natl Acad Sci U S A 2010;107:7892–7897.
[32] **Ramos MJ**, **Bandiera L**, Menolascina F, et al. In vitro models for non-alcoholic fatty liver disease: emerging platforms and their applications. iScience 2022;25:103549.
[33] Loomba R, Friedman SL, Shulman GI. Mechanisms and disease consequences of nonalcoholic fatty liver disease. Cell 2021;184:2537–2564.
[34] Mazza G, Al-Akkad W, Rombouts K. Engineering in vitro models of hepatofibrogenesis. Adv Drug Deliv Rev 2017;121:147–157.
[35] Mazza G, Al-Akkad W, Telese A, et al. Rapid production of human liver scaffolds for functional tissue engineering by high shear stress oscillation-decellularization. Sci Rep 2017;7:5534.
[36] Mazza G, Telese A, Al-Akkad W, et al. Cirrhotic human liver extracellular matrix 3D scaffolds promote smad-dependent TGF-beta1 epithelial mesenchymal transition. Cells 2019;9.
[37] Thanapirom K, Caon E, Papatheodoridi M, et al. Optimization and validation of a novel three-dimensional Co-culture system in decellularized human liver scaffold for the study of liver fibrosis and cancer. Cancers (Basel) 2021;13.
[38] **Baselli GA**, **Dongiovanni P**, Rametta R, et al. Liver transcriptomics highlights interleukin-32 as novel NAFLD-related cytokine and candidate biomarker. Gut 2020;69:1855–1866.
[39] Kleiner DE, Brunt EM, Van Natta M, et al. Design and validation of a histological scoring system for nonalcoholic fatty liver disease. Hepatology 2005;41:1313–1321.
[40] **Rombouts K**, **Carloni V**. Determination and characterization of tetraspanin-associated phosphoinositide-4 kinases in primary and neoplastic liver cells. Methods Mol Biol 2016;1376:203–212.
[41] Samarakoon R, Higgins PJ. Integration of non-SMAD and SMAD signaling in TGF-beta1-induced plasminogen activator inhibitor type-1 gene expression in vascular smooth muscle cells. Thromb Haemost 2008;100:976–983.
[42] **Begliuomini C**, **Magli G**, Di Rocco M, et al. VARS2-linked mitochondrial encephalopathy: two case reports enlarging the clinical phenotype. BMC Med Genet 2019;20:77.
[43] Mick E, Titov DV, Skinner OS, et al. Distinct mitochondrial defects trigger the integrated stress response depending on the metabolic state of the cell. Elife 2020;9.
[44] Kayvanpour E, Wisdom M, Lackner MK, et al. VARS2 depletion leads to activation of the integrated stress response and disruptions in mitochondrial fatty acid oxidation. Int J Mol Sci 2022:23.
[45] Kim JA, Wei Y, Sowers JR. Role of mitochondrial dysfunction in insulin resistance. Circ Res 2008;102:401–414.
[46] Liu RM, Desai LP. Reciprocal regulation of TGF-beta and reactive oxygen species: a perverse cycle for fibrosis. Redox Biol 2015;6:565–577.
[47] Pols TW, Ottenhoff R, Vos M, et al. Nur77 modulates hepatic lipid metabolism through suppression of SREBP1c activity. Biochem Biophys Res Commun 2008;366:910–916.
[48] **Xu Y**, **Tian J**, Kang Q, et al. Knockout of Nur77 leads to amino acid, lipid, and glucose metabolism disorders in zebrafish. Front Endocrinol (Lausanne) 2022;13:864631.
[49] Lee SO, Jin UH, Kang JH, et al. The orphan nuclear receptor NR4A1 (Nur77) regulates oxidative and endoplasmic reticulum stress in pancreatic cancer cells. Mol Cancer Res 2014;12:527–538.
[50] Palumbo-Zerr K, Zerr P, Distler A, et al. Orphan nuclear receptor NR4A1 regulates transforming growth factor-beta signaling and fibrosis. Nat Med 2015;21:150–158.
[51] **Xiong Y**, **Ran J**, **Xu L**, et al. Reactivation of NR4A1 restrains chondrocyte inflammation and ameliorates osteoarthritis in rats. Front Cell Dev Biol 2020;8:158.
[52] Zhan Y, Du X, Chen H, et al. Cytosporone B is an agonist for nuclear orphan receptor Nur77. Nat Chem Biol 2008;4:548–556.
[53] **Zeng X**, **Yue Z**, Gao Y, et al. NR4A1 is involved in fibrogenesis in ovarian endometriosis. Cell Physiol Biochem 2018;46:1078–1090.
[54] Yang J, Trepo E, Nahon P, et al. PNPLA3 and TM6SF2 variants as risk factors of hepatocellular carcinoma across various etiologies and severity of underlying liver diseases. Int J Cancer 2019;144:533–544.
[55] Zhang C, Zhao Y, Yu M, et al. Mitochondrial dysfunction and chronic liver disease. Curr Issues Mol Biol 2022;44:3156–3165.
[56] Begriche K, Igoudjil A, Pessayre D, et al. Mitochondrial dysfunction in NASH: causes, consequences and possible means to prevent it. Mitochondrion 2006;6:1–28.

[57] Teodoro JS, Rolo AP, Duarte FV, et al. Differential alterations in mitochondrial function induced by a choline-deficient diet: understanding fatty liver disease progression. Mitochondrion 2008;8:367–376.
[58] Koliaki C, Szendroedi J, Kaul K, et al. Adaptation of hepatic mitochondrial function in humans with non-alcoholic fatty liver is lost in steatohepatitis. Cell Metab 2015;21:739–746.
[59] Lev D, Gilad E, Leshinsky-Silver E, et al. Reversible fulminant lactic acidosis and liver failure in an infant with hepatic cytochrome-c oxidase deficiency. J Inherit Metab Dis 2002;25:371–377.
[60] Min HK, Sookoian S, Pirola CJ, et al. Metabolic profiling reveals that PNPLA3 induces widespread effects on metabolism beyond triacylglycerol remodeling in Huh-7 hepatoma cells. Am J Physiol Gastrointest Liver Physiol 2014;307:G66–G76.
[61] Perez-Carreras M, Del Hoyo P, Martin MA, et al. Defective hepatic mitochondrial respiratory chain in patients with nonalcoholic steatohepatitis. Hepatology 2003;38:999–1007.
[62] **Chimienti G**, **Orlando A**, Russo F, et al. The mitochondrial trigger in an animal model of nonalcoholic fatty liver disease. Genes (Basel) 2021;12.
[63] Lee YI, Hwang JM, Im JH, et al. Human hepatitis B virus-X protein alters mitochondrial function and physiology in human liver cells. J Biol Chem 2004;279:15460–15471.
[64] Aharoni-Simon M, Hann-Obercyger M, Pen S, et al. Fatty liver is associated with impaired activity of PPARgamma-coactivator 1alpha (PGC1alpha) and mitochondrial biogenesis in mice. Lab Invest 2011;91:1018–1028.
[65] Middleton P, Vergis N. Mitochondrial dysfunction and liver disease: role, relevance, and potential for therapeutic modulation. Therap Adv Gastroenterol 2021;14:17562848211031394.
[66] Masarone M, Rosato V, Dallio M, et al. Role of oxidative stress in pathophysiology of nonalcoholic fatty liver disease. Oxid Med Cell Longev 2018;2018:9547613.
[67] Kushnareva Y, Murphy AN, Andreyev A. Complex I-mediated reactive oxygen species generation: modulation by cytochrome c and NAD(P)+ oxidation-reduction state. Biochem J 2002;368:545–553.
[68] Hruszkewycz AM, Bergtold DS. The 8-hydroxyguanine content of isolated mitochondria increases with lipid peroxidation. Mutat Res 1990;244:123–128.
[69] Parola M, Pinzani M, Casini A, et al. Stimulation of lipid peroxidation or 4-hydroxynonenal treatment increases procollagen alpha 1 (I) gene expression in human liver fat-storing cells. Biochem Biophys Res Commun 1993;194:1044–1050.
[70] Chen J, Schenker S, Frosto TA, et al. Inhibition of cytochrome c oxidase activity by 4-hydroxynonenal (HNE). Role of HNE adduct formation with the enzyme subunits. Biochim Biophys Acta 1998;1380:336–344.
[71] Zamara E, Novo E, Marra F, et al. 4-Hydroxynonenal as a selective profibrogenic stimulus for activated human hepatic stellate cells. J Hepatol 2004;40:60–68.
[72] Chambel SS, Santos-Goncalves A, Duarte TL. The dual role of Nrf2 in nonalcoholic fatty liver disease: regulation of antioxidant defenses and hepatic lipid metabolism. Biomed Res Int 2015;2015:597134.
[73] Besse-Patin A, Leveille M, Oropeza D, et al. Estrogen signals through peroxisome proliferator-activated receptor-gamma coactivator 1alpha to reduce oxidative damage associated with diet-induced fatty liver disease. Gastroenterology 2017;152:243–256.
[74] **Okina Y**, **Sato-Matsubara M**, Matsubara T, et al. TGF-beta1-driven reduction of cytoglobin leads to oxidative DNA damage in stellate cells during non-alcoholic steatohepatitis. J Hepatol 2020;73:882–895.
[75] Pingitore P, Dongiovanni P, Motta BM, et al. PNPLA3 overexpression results in reduction of proteins predisposing to fibrosis. Hum Mol Genet 2016;25:5212–5222.
[76] Dewidar B, Meyer C, Dooley S, et al. TGF-Beta in hepatic stellate cell activation and liver fibrogenesis-updated 2019. Cells 2019;8.
[77] Uhlen M, Oksvold P, Fagerberg L, et al. Towards a knowledge-based human protein Atlas. Nat Biotechnol 2010;28:1248–1250.
[78] Claveria-Cabello A, Colyn L, Uriarte I, et al. Dual pharmacological targeting of HDACs and PDE5 inhibits liver disease progression in a mouse model of biliary inflammation and fibrosis. Cancers (Basel) 2020;12.
[79] Biswas S, Yadav N, Juneja P, et al. Conformationally restricted dipeptide-based nanoparticles for delivery of siRNA in experimental liver cirrhosis. ACS Omega 2022;7:36811–36824.
[80] Huang Q, Xu J, Ge Y, et al. NR4A1 inhibits the epithelial-mesenchymal transition of hepatic stellate cells: involvement of TGF-beta-Smad2/3/4-ZEB signaling. Open Life Sci 2022;17:447–454.
[81] **Geng N**, **Chen T**, **Chen L**, et al. Nuclear receptor Nur77 protects against oxidative stress by maintaining mitochondrial homeostasis via regulating mitochondrial fission and mitophagy in smooth muscle cell. J Mol Cell Cardiol 2022;170:22–33.
[82] Venu VKP, Saifeddine M, Mihara K, et al. Metformin prevents hyperglycemia-associated, oxidative stress-induced vascular endothelial dysfunction: essential role for the orphan nuclear receptor human nuclear receptor 4A1 (Nur77). Mol Pharmacol 2021;100:428–455.
[83] **Wang D**, **Yin Y**, **Wang S**, et al. FGF1(DeltaHBS) prevents diabetic cardiomyopathy by maintaining mitochondrial homeostasis and reducing oxidative stress via AMPK/Nur77 suppression. Signal Transduct Target Ther 2021;6:133.
[84] Zheng Y, Tao Y, Zhan X, et al. Nuclear receptor 4A1 (NR4A1) silencing protects hepatocyte against hypoxia-reperfusion injury in vitro by activating liver kinase B1 (LKB1)/AMP-activated protein kinase (AMPK) signaling. Bioengineered 2022;13:8349–8359.
[85] **Zhou F**, **Bai M**, Zhang Y, et al. Berberine-induced activation of AMPK increases hepatic FGF21 expression via NUR77. Biochem Biophys Res Commun 2018;495:1936–1941.
[86] Su H, Haque M, Becker S, et al. Long-term hypercaloric diet exacerbates metabolic liver disease in PNPLA3 I148M animals. Liver Int 2023;43:1699–1713.
[87] **Volkert I**, **Fromme M**, Schneider C, et al. Impact of PNPLA3 I148M on alpha-1 antitrypsin deficiency-dependent liver disease progression. Hepatology 2024 Apr 1;79(4):898–911. https://doi.org/10.1097/HEP.0000000000000574.
[88] Cherubini A, Ostadreza M, Jamialahmadi O, et al. Interaction between estrogen receptor-alpha and PNPLA3 p.I148M variant drives fatty liver disease susceptibility in women. Nat Med 2023;29:2643–2655.